Cancer Research

Novel Matrix Metalloproteinase Inhibitor [^{18}F]Marimastat-Aryltrifluoroborate as a Probe for *In vivo* Positron Emission Tomography Imaging in Cancer

Ulrich auf dem Keller[1], Caroline L. Bellac[1], Ying Li[2], Yuanmei Lou[4], Philipp F. Lange[1], Richard Ting[2], Curtis Harwig[2], Reinhild Kappelhoff[1], Shoukat Dedhar[4], Michael J. Adam[2,6], Thomas J. Ruth[2,3], François Bénard[5], David M. Perrin[2], and Christopher M. Overall[1]

Abstract

Matrix metalloproteinases (MMP), strongly associated pathogenic markers of cancer, have undergone extensive drug development programs. Marimastat, a noncovalent MMP inhibitor, was conjugated with FITC to label cellular metalloproteinase cancer targets in MDA-MB-231 cells *in vitro*. Punctate localization of active transmembrane MMP14 was observed. For molecular-targeted positron emission tomography imaging of syngeneic 67NR murine mammary carcinoma *in vivo*, marimastat was ^{18}F-labeled using a shelf-stable arylboronic ester conjugate as a captor for aqueous [^{18}F]fluoride in a novel, rapid one-step reaction at ambient temperature. [^{18}F]Marimastat-aryltrifluoroborate localized to the tumors, with labeling being blocked in control animals first loaded with >10-fold excess unlabeled marimastat. The labeled drug cleared primarily via the hepatobiliary and gastrointestinal tract, with multiple animals imaged in independent experiments, confirming the ease of this new labeling strategy. *Cancer Res; 70(19); 7562–9. ©2010 AACR.*

Introduction

Positron emission tomography (PET) for molecular imaging is one of the most powerful noninvasive imaging technologies for the production of high-resolution, three-dimensional images within deep tissue needed for human clinical application (1). Fluorine-18 (^{18}F) is the optimal PET radioisotope because of its short half-life leading to favorable radiometric dosimetry, its high sensitivity, and the ability to quantify tissue distribution of conjugated compounds. Indeed, [^{18}F]-2-deoxy-D-glucose (FDG) is the most widely used radiotracer for cancer diagnostics despite a relative lack of target specificity (1). Hence, cancer-specific small molecule ^{18}F-labeled radiotracers are urgently needed.

Rapid on-site production of bioactive specific molecular imaging agents is hampered by ^{18}F labeling methodologies that traditionally have relied on C–F bond formation under conditions that are generally incompatible with biomolecule stability, such as scrupulously dry organic solvents at 70°C to 140°C. Overcoming these obstacles is plagued by relatively time-consuming multistep syntheses that are further complicated by side reactions requiring extensive purification. Coupled with the short half-life of ^{18}F (110 min), these problems reduce specific activity and the imaging time window. Recently, Ting and colleagues (2) used arylboronate precursors to capture aqueous [^{18}F]fluoride in the form of an aryltrifluoroborate ($ArBF_3$) for ^{18}F-labeling in a rapid, one-step synthesis under acidic aqueous conditions at room temperature. Indeed, the [^{18}F]aryltrifluoroborate was stable *in vivo* because no [^{18}F]fluoride accumulation was detected in bone, a highly fluorophilic tissue (3). Such chemistries have the potential to fast-track the introduction of ^{18}F-labeled bioconjugates in "kit" form[7] for diagnostic imaging in humans.

To validate this novel labeling method for cancer imaging, we hypothesized that an optimal target would be highly expressed in many tumors, show discrimination between different cancer stages, and be targeted by nanomolar inhibitor drugs with clinically demonstrated safety. These criteria are met by matrix metalloproteinases (MMP) that are expressed

Authors' Affiliations: [1]UBC Centre for Blood Research, Departments of Oral Biological and Medical Sciences, and Biochemistry and Molecular Biology, [2]Chemistry, and [3]Medicine, University of British Columbia; [4]Department of Cancer Genetics and [5]Molecular Oncology Department, BC Cancer Agency Research Centre; and [6]PET Chemistry Group, TRIUMF, Vancouver, British Columbia, Canada

Note: Supplementary data for this article are available at Cancer Research Online (http://cancerres.aacrjournals.org/).

Present address for U. auf dem Keller: Institute of Cell Biology, ETH Zurich, Schafmattstr. 18, CH-8093 Zurich, Switzerland.

U. auf dem Keller and C.L. Bellac contributed equally to this work.

D.M. Perrin and C.M. Overall shared senior authorship.

Corresponding Authors: Christopher M. Overall, University of British Columbia, 2350 Health Sciences Mall, Vancouver, British Columbia, Canada V6T 1Z3. Phone: 604-822-2958; Fax: 604-822-7742; E-mail: chris.overall@ubc.ca and David M. Perrin, Phone: 604-822-0567; Fax: 604-822-2847; E-mail: dperrin@chem.ubc.ca.

doi: 10.1158/0008-5472.CAN-10-1584

[7] Li Y, Ting R, Harwig C, et al. Kit-like ^{18}F-labeling of small molecules with specific activities suitable for *in vivo* PET imaging: toward imaging cancer associated matrix metalloproteases. 2010; submitted for publication.

and activated in most cancers and their peritumor stroma (4, 5). With many MMP inhibitor drug candidates reaching phase III clinical trials, their failure has nevertheless been disappointing (4, 6). Marimastat, a nanomolar hydroxamate peptidic broad-spectrum MMP inhibitor (7) with activity against related MMPs, such as the ADAMs and ADAMTSs that are also often associated with cancer (4, 5), is a noncovalent and thereby reversible inhibitor, and thus has reduced potential for tissue accumulation and unwanted irreversible side reactions in short-term imaging applications. In late phase III clinical trials involving thousands of patients with advanced cancer, including breast carcinoma trials, marimastat proved to be safe, although some patients reported musculoskeletal pain (7). Hence, we selected marimastat as a scaffold onto which a boronic acid could be grafted for aqueous [^{18}F]fluoride capture so as to develop a noninvasive, clinically safe radiotracer for the *in vivo* imaging of cancer by detection of elevated MMP levels. We present the first one-step radiolabeling for *in vivo* application of a molecular-targeted [^{18}F]-PET probe for cancer detection and show high specificity labeling of mammary carcinomas in mice.

Materials and Methods

Cell lines

MDA-MB-231 breast carcinoma cells were kindly provided by Dr. V.C. Jordan (Northwestern University, Chicago, IL) in 2002. Stable MMP14 transfectants were established and characterized by us as described previously (8, 9). The murine breast cancer cell line, 67NR (10), was kindly provided by Dr. Fred Miller (Karmanos Cancer Institute, Detroit, MI) in July 2008. The cell line was authenticated for growth *in vitro* and *in vivo* as described by us previously (11).

Syngeneic tumor model

Female BALB/c mice (7–9 weeks old; Taconic Laboratories) were injected with 1×10^6 viable 67NR/CMV-Luciferase murine mammary cancer cells into the right fourth mammary gland (50 μL in PBS per mouse; ref. 11).

Microarray analysis

Primary syngeneic 67NR tumor tissues and control mammary glands were dissected by laser capture microdissection (11). Total cellular RNA was extracted using RNeasy (Qiagen) and re-extracted and resuspended in 10 μL of diethylpyrocarbonate-treated water. RNA was quantified and qualified using an Agilent 2100 Bioanalyzer. RNA probes were labeled and hybridized to the CLIP-CHIP^{TM} (12), a dedicated murine protease and inhibitor DNA microarray. Data were analyzed using the R Bioconductor package with CARMAweb 1.3 front-end. Spot intensities were background-corrected using the "normexp" method and data normalized within and between arrays by applying print-tip loess and quantile normalization, respectively (12). For statistical analysis, moderated *t* statistics (Bioconductor "limma" package) were used and *P* values calculated using Benjamini-Hochberg correction for multiple testing.

Chemical synthesis

Chemicals were purchased from Sigma-Aldrich and Acros Organics. Deuterated solvents were purchased from Cambridge Isotope Laboratories. Analytic and preparative TLC were performed using Silica Gel 60 F_{254} Glass TLC plates from EMD Chemicals. All ^{1}H-nuclear magnetic resonance (NMR) spectra were recorded on a Bruker Avance 300 or 400 MHz instrument. Chemical shifts are reported using the δ scale in ppm and all coupling constants (*J*) are reported in hertz (Hz). Unless specified, ^{1}H-NMR spectra are referenced to the tetramethylsilane peak (δ = 0.00) and ^{19}F-NMR spectra are referenced to NEAT trifluoroacetic acid (δ = 0.00, −78.3 ppm relative to $CFCl_3$). Due to the presence of ^{19}F contaminations in the NMR spectrometer probe, baseline corrections for samples <20 mmol/L in ^{19}F concentration had to be adjusted by multipoint linear baseline correction using MestReC 4.9.9.9. This correction did not affect the absolute chemical shifts or integration ratios of ^{19}F signals.

Final synthesis of compounds illustrated in Fig. 2A is described below. Synthesis of precursor compounds is fully detailed in Supplementary Materials and Methods (Note: if not specifically indicated, compound numbers refer to Supplementary Schemes 1 to 4).

Marimastat

(2R,3S)-N^1-((S)-3,3-dimethyl-1-(methylamino)-1-oxobutan-2-yl)-N^4,3-dihydroxy-2-isobutylbutanediamide (1). To a solution of methyl ester **5** (92 mg, 0.28 mmol) in methanol/THF (1:1, 0.8 mL) was added KCN (3 mg) followed by a solution of hydroxylamine in H_2O (50 wt%, 100 μL, 1.5 mmol) and the reaction stirred at room temperature for 16 hours. The mixture was then concentrated under reduced pressure and diluted with CH_2Cl_2/methanol (19:1, 2 × 10 mL). The CH_2Cl_2/methanol washings were filtered and concentrated under reduced pressure to afford marimastat (**1**, 77 mg, 83%) as a white solid. ^{1}H-NMR (400 MHz, CD_3OD) δ 4.19 (s, ^{1}H), 4.01 (d, *J* = 6.3 Hz, ^{1}H), 2.82 to 2.79 (m, ^{1}H), 2.73 (s, 3H), 1.62 to 1.53 (m, 2H), 1.31 to 1.28 (m, ^{1}H), 1.01 (s, 9H), 0.92 (d, *J* = 6.5 Hz, 3H), 0.89 (d, *J* = 6.5 Hz, 3H); ^{13}C-NMR (100 MHz, CD_3OD) δ 176.1, 173.5, 169.7, 73.4, 62.5, 50.0, 39.9, 35.5, 27.4, 27.1, 26.3, 23.8, 22.6; HRMS (ESI) calculated for $C_{15}H_{29}N_3O_5Na^+$ $(M + Na)^+$ 354.2005, found 354.2002 (Marimastat; Fig. 2A, **1**).

Marimastat-linker

(15S,18R,19S)-Methyl 15-tert-butyl-19-hydroxy-18-isobutyl-3,14,17-trioxo-1-phenyl-2,7,10-trioxa-4,13,16-triazaicosan-20-oate (11). To a solution of acetonide **10** (0.90 g, 1.48 mmol) in anhydrous methanol (25 mL) was added *p*-TsOH·H_2O (63 mg) and the mixture heated to reflux for 70 minutes. The reaction was then concentrated and diluted with CH_2Cl_2 (40 mL) and brine (20 mL). The layers were separated and the aqueous phase was extracted with CH_2Cl_2 (2 × 10 mL). The combined organic extracts were dried (Na_2SO_4) and purified by column chromatography on silica gel (CH_2Cl_2/methanol, 98:2 then 95:5) to afford methyl ester **11** (0.71 g, 83%) as a white foam. ^{1}H-NMR (300 MHz, $CDCl_3$) δ 7.35 to 7.29 (m, 5H), 6.58 (br d, *J* = 6.7 Hz, ^{1}H), 6.45 (m, ^{1}H), 5.50 (m, ^{1}H), 5.10 (s, 2H), 4.27 to 4.21 (m, 2H), 4.16 (br d, *J* = 6.8 Hz, ^{1}H),

3.74 (s, 3H), 3.59 to 3.37 (m, 12H), 2.82 (m, ^{1}H), 1.66 to 1.55 (m, 3H), 0.96 (s, 9H), 0.92 (d, J = 6.0 Hz, 3H), 0.91 (d, J = 6.0 Hz, 3H); ^{13}C-NMR (100 MHz, $CDCl_3$) δ 173.7, 173.2, 170.1, 156.5, 136.4, 128.4, 128.0, 71.7, 70.1, 70.1, 69.9, 69.5, 66.5, 60.5, 52.3, 47.2, 40.7, 39.1, 38.4, 34.4, 26.5, 25.4, 22.4, 22.4; HRMS (ESI) calculated for $C_{29}H_{47}N_3O_9Na^+$ $(M + Na)^+$ 604.3210, found 604.3212 (Marimastat-linker; Fig. 2A, **2**).

Marimastat-FITC

(13S,16R,17S)-Methyl 13-tert-butyl-1-(3′,6′-dihydroxy-3-oxo-3H-spiro[isobenzofuran-1,9′-xanthene]-5(6)-ylamino)-17-hydroxy-16-isobutyl-12,15-dioxo-1-thioxo-5,8-dioxa-2,11,14-triazaoctadecan-18-oate (13). To a solution of Cbz-protected **11** (28 mg, 0.048 mmol) in methanol (4.5 mL) was added Pd/C (10%, 6.5 mg) and the mixture stirred under an atmosphere of H_2(g) (balloon) for 1 hour. The reaction was then filtered through Celite, washing with methanol and CH_2Cl_2. The combined filtrate was concentrated under reduced pressure and used immediately in the next reaction. To a solution of the resultant amine **12** in anhydrous DMF (2 mL) was added fluorescein 5(6)-isothiocyanate (90%, 18.5 mg, 0.043 mmol) and the reaction stirred for 1.5 hours. The mixture was then concentrated and purified by chromatography on silica gel (CH_2Cl_2/methanol/AcOH, 95:5:0 then 9:1:0 then 89:10:1) to afford the desired fluorescein derivative **13** (23 mg, 58% over two steps) as a yellow oil (mixture of regioisomers). HRMS (ESI) calculated for $C_{42}H_{51}N_4O_{12}S^-$ $(M - H)^-$ 835.3224, found 835.3241.

(2R,3S)-N^1-((S)-1-(3′,6′-dihydroxy-3-oxo-3H-spiro[isobenzofuran-1,9′-xanthene]-6-ylamino)-14,14-dimethyl-12-oxo-1-thioxo-5,8-dioxa-2,11-diazapentadecan-13-yl)-N^4,3-dihydroxy-2-isobutylbutanediamide (14). To a solution of the methyl ester **13** (10 mg, 0.012 mmol) in methanol/THF (1:1, 0.8 mL) was added KCN (~1 mg) followed by a solution of hydroxylamine in H_2O (50 wt%, 100 μL, 1.5 mmol) and the reaction stirred at room temperature for 16 hours. The mixture was then concentrated under reduced pressure and triturated with CH_2Cl_2/methanol (5:1, 3 × 5 mL). The CH_2Cl_2/methanol washings were filtered and concentrated under reduced pressure to afford the desired hydroxamate **14** (9 mg, 90%) as an orange solid (mixture of regioisomers). HRMS (ESI) calculated for $C_{41}H_{51}N_5O_{12}SNa^+$ $(M + Na)^+$ 860.3153, found 860.3134 (Marimastat-FITC; Fig. 2A, 3).

Marimastat-boronate and marimastat-ArBF$_3$

The radiochemical synthesis of marimastat-boronate and marimastat-ArBF$_3$ (Fig. 2A, 4, and 5) are fully detailed in Li and colleagues.[7] For an outline of the chemistry applied, see Supplementary Scheme 4(Fig. 2A, **4** and **5**).

Inhibitor kinetics

Recombinant human MMP2 (13) was activated with 1 mmol/L of 4-aminophenylmercuric acetate for 1 hour at 37°C. Rates of cleavage of 1 μmol/L of the quenched fluorescent MMP substrate (7-methoxycoumarin-4-yl)acetyl-Pro-Leu-Gly-Leu-[3-(2,4-dinitrophenyl)-L-2,3-diaminoproprionyl]-Ala-Arg-NH_2 were measured in 96-well fluorimetry plates in a Polarstar Optima (BMG Labtech GmbH) at 37°C 100 mmol/L Tris-HCl (pH 7.5), 100 mmol/L NaCl, 10 mmol/L $CaCl_2$, 0.05% Brij 35 using a 320-nm excitation filter and a 405-nm emission filter in the presence of increasing inhibitor concentrations. Curve-fitting and IC_{50} calculations were done using GraphPad Prism 5.0 Software (GraphPad Software).

Marimastat-FITC as a MMP activity–based probe

Recombinant human MMP2, 8, 9, 13, and 14 (also known as membrane type 1-MMP) were expressed and purified. 4-Aminophenylmercuric acetate–activated MMPs were resolved nonreduced on a 10% SDS-PAGE gel. SDS was removed using Triton X-100 washes and renatured proteins in the gels were incubated overnight with 1 μmol/L of marimastat-FITC in 100 mmol/L Tris, 30 mmol/L $CaCl_2$ (pH 8), 37°C. After washing three times (10 min) with PBS and imaging the gels using a 340-nm excitation filter on an Alpha Imager system (Alpha Innotech), they were stained with Coomassie brilliant blue R250. For assessing active MMPs in primary 67NR mammary tumors (11) and control mammary gland, the tissues were homogenized in 100 mmol/L of Tris, 30 mmol/L of $CaCl_2$, 0.05% Brij 35 (pH 8). Extracts were clarified (14,000 × g) and 100 μg of total protein in supernatants were resolved on a 10% SDS-PAGE gel and processed for marimastat-FITC imaging.

Marimastat-FITC visualization of MMP14 in cell culture

MDA-MB-231 stably transfected with human MMP14 (with a FLAG-tag in the juxtamembrane stalk) or empty vector (8) were cultured in DMEM, 10% fetal bovine serum with G418 selection (Geneticin, 1 mg/mL; Life Technologies, Invitrogen Canada). For MMP14 activity-staining, the cells were grown on glass chamber slides and incubated with 20 μmol/L of marimastat-FITC in culture medium for 12 hours. The cells were then washed twice with PBS, counterstained with Hoechst (0.1 mg/mL in PBS, 20 min, at 25°C), and fixed for 20 minutes with 4% formalin. The slides were washed two times with PBS, mounted in ProLong Gold antifade reagent (Invitrogen Life Technologies) and imaged using a Leica DMRA2 fluorescence microscope. Pictures were taken with a 100× oil immersion objective with the same exposure time and digital gain for MMP14-transfected and vector control cells.

PET imaging of tumors *in vivo*

Day 25 67NR tumors were imaged by *in vivo* bioluminescence on a cryogenically cooled IVIS system (Xenogen Corporation) using Living Imaging acquisition and Living Image 2.50.1 software analysis (11). One day after IVIS imaging (day 26 or 33) control 67NR tumor mice were injected i.p. with blocking solution [300 nmol marimastat (**1**) in PBS], three times over 60 minutes prior to tracer injection. Pre-blocked and unblocked mice were then anesthetized with isoflurane (5% induction, 1.5% maintenance), and injected (tail vein)

[7] Li Y, Ting R, Harwig C, et al. Kit-like ^{18}F-labeling of small molecules with specific activities suitable for *in vivo* PET imaging: toward imaging cancer associated matrix metalloproteases. 2010; submitted for publication.

with 50 to 100 μCi ^{18}F-labeled marimastat-ArBF$_3$ (**5**; decay-corrected specific activity of 0.185 Ci/μmol or 0.39 Ci/μmol at the time of injections) or 440 μCi control-ArBF$_3$ (Supplementary data, **15**) prepared as described in Supplementary data and Li and colleagues.[7] Five minutes later, animals underwent an 80-minute dynamic scan followed by a 10-minute transmission scan using a microPET Focus 120 (CTI Concorde) system. Groups of mice were imaged with ^{18}F-labeled marimastat-ArBF$_3$ on three separate occasions with or without prior blocking with the underivatized marimastat. PET data were compiled with Siemens Focus 120 microPET software. PET images and time–activity curves were generated with Amide version 0.8.19.

Results

MMP expression patterns differed between mammary control tissues (n = 3) and tumors (n = 3; Fig. 1) where transcripts of MMP7, 13, 14, and 24 were statistically significantly elevated (P < 0.05), but others were reduced compared with normal tissue including MMP2, 15, 23, 25, and 27. Hence, 67NR tumor-expressed MMPs were probed with marimastat conjugates.

Marimastat (**1**; Fig. 2A) was synthesized as a reference for inhibitory activity of imaging derivatives. We then synthesized a highly versatile derivative precursor by the addition of a linker

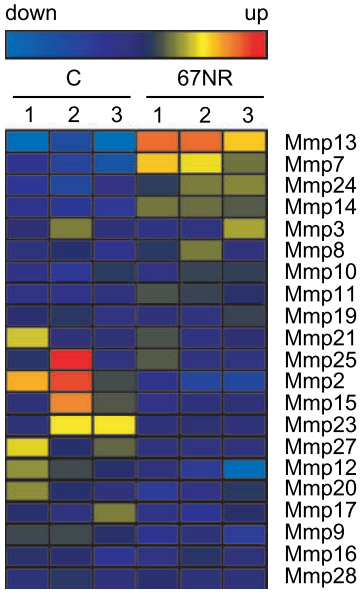

Figure 1. High expression of MMPs in primary 67NR mammary tumors. Total RNA isolated from normal mammary glands of three individual control mice (C 1, 2, 3) and from primary tumors of three individual mice (67NR 1, 2, 3) were analyzed by CLIP-CHIP™ microarray in a two-color experiment with universal mouse RNA as control. The expression maps are derived from log$_2$-ratios (tumor or control/universal mouse RNA) with red representing genes highly upregulated and light blue highly downregulated in comparison to universal mouse RNA.

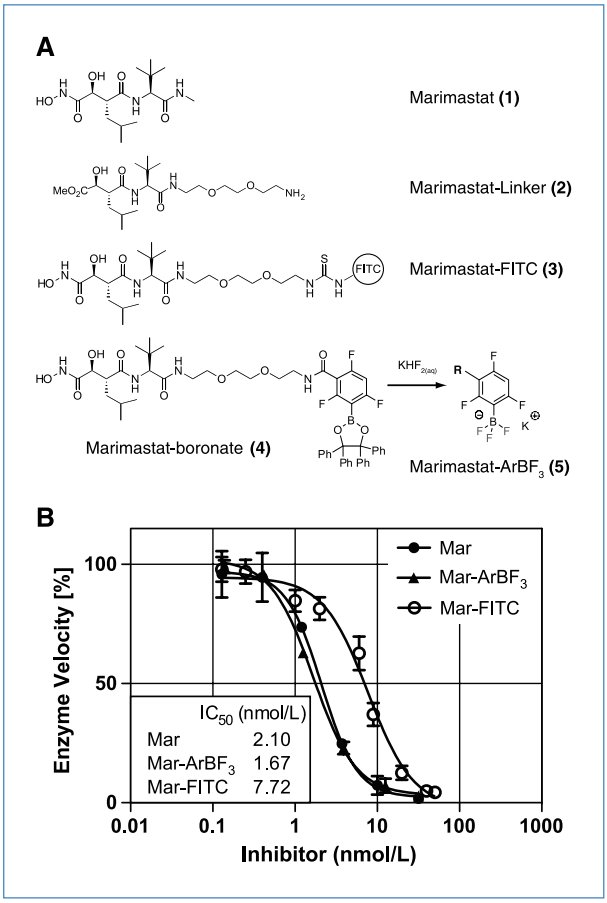

Figure 2. One-step radiolabeling and bioactivity of marimastat derivatives. A, panel of compounds used in this study and one-step fluorination scheme for marimastat-boronate (**4**). B, inhibitor kinetics of marimastat derivatives. MMP2 (5 pmol/mL) was incubated for 20 min with a quenched fluorescent peptidic substrate (1 μmol/L) in the presence of various inhibitor concentrations.

arm at the P3′ site, which is known not to interfere with potency or specificity (ref. 14; marimastat-linker, **2**). This was used as an attachment point for generating a fluorescent imaging probe (marimastat-FITC, **3**) and a shelf-stable marimastat-arylboronic ester conjugate (marimastat-boronate, **4**). For PET imaging, marimastat-boronate(**4**) is converted in a single step to marimastat-ArBF$_3$ (**5**) under aqueous conditions at ambient temperature (18°C) and isolated in radiochemically pure form as described in Li and colleagues.[7]

With an IC$_{50}$ of 2.10 nmol/L (Fig. 2B) and in good agreement with original reports (7), marimastat (**1**), was a nmol/L inhibitor against MMP2, an important protease in tumor angiogenesis and breast cancer metastases (15). Marimastat-ArBF$_3$ (**5**) showed the same IC$_{50}$ (1.67 nmol/L), with marimastat-FITC (**3**) having a value only slightly higher

[7] Li Y, Ting R, Harwig C, et al. Kit-like ^{18}F-labeling of small molecules with specific activities suitable for *in vivo* PET imaging: toward imaging cancer associated matrix metalloproteases. 2010; submitted for publication.

(Fig. 2B). Following SDS-PAGE marimastat-FITC (**3**) specifically labeled activated MMP2, 9, 13, and 14 despite stringent washes (Fig. 3A and B) alleviating a concern that its dissociation rate might interfere with planned MMP detection *in vivo*. Neither the molecular weight markers nor the autolytically cleaved hemopexin domain of MMP13 showed labeling, confirming active site specificity. Notably, similar analysis of murine tissue lysates with marimastat-FITC (**3**) revealed MMP activity in the tumors ($n = 2$) greatly exceeding that observed in control mammary gland tissue ($n = 2$; Fig. 3B).

We next established *in vitro* imaging efficacy. Human MDA-MB-231 breast carcinoma cells stably expressing MMP14, a transmembrane protease highly expressed in cancer that activates proMMP2, but not vector transfectant controls were specifically labeled with marimastat-FITC (**3**; Fig. 3C). The punctate localization of MMP14 on the plasma membrane correlates with immunofluorescence studies or when GFP-MMP14 was expressed in the same cells (16).

Primary tumors were imaged over 25 days by luciferase bioluminescence (Fig. 4A, left). For PET molecular imaging of MMPs *in vivo*, separate radiosyntheses of marimastat-$ArBF_3$ (**5**) were performed that afforded ~1 mCi of **5** with respective specific activities of 0.185 Ci/μmol for imaging on day 26 and 0.39 Ci/μmol for imaging on day 33. Sixty minutes after the injection of tumor-bearing mice with 50 to 100 μCi of marimastat-$ArBF_3$ (**5**), we observed low but detectable and specific uptake in the primary tumor, whereas in mice injected with 440 μCi control-$ArBF_3$ (Supplementary data, **15**) lacking the marimastat moiety no tumor localization was observed, with clearance only to the liver, bladder, and submaxillary salivary gland (Fig. 4A). As a further specificity control, we preblocked tumor-bearing mice with 300 nmol of unlabeled marimastat (**1**) prior to the tracer injection. The preblocked mice had clearly reduced activity in the same region as the littermates with similarly sized tumors (Fig. 4B and C). A small amount of bone uptake was seen due to the presence of ~3% to 5% free [^{18}F]fluoride that may have coeluted with the sample during the chromatographic separation and/or possibly solvolyzed on standing. Time–activity curve analysis revealed that marimastat-$ArBF_3$ (**5**) accumulated in the tumor at 60 minutes (Fig. 4D). Overall, the PET imaging and time–activity curve analyses show specific ^{18}F-labeling of the tumor as well as of bladder, liver, stomach, and gut to which the compound cleared (Supplementary Fig. S1).

Discussion

The use of a noncovalent nanomolar protease inhibitor drug as a model bioconjugate shows the ease and broad applicability of this novel labeling technique for *in vivo* cancer imaging. Previously, metalloproteinase activity has been imaged in mouse models of cancer by fluorescent detection of cleaved peptides quenched with near-IR fluorochromes, but this approach suffers from low tissue penetrance and does not afford deep tissue localization (17).

In contrast, using small molecule drugs offers improved pharmacokinetics and biodistribution in solid tumors. For some serine and cysteine proteases, covalent inhibitors for imaging can be used (18), but for metalloproteinases, only noncovalent inhibitors are available for *in vivo* application. Nonetheless, this approach has advantages including reduced probe accumulation in tissues that can lead to unwanted side reactions. Together with rapid clearance, this also circumvents the long time intervals needed to reduce background from unincorporated covalent probes in tissues before imaging.

Although [^{11}C]methylation represents an attractive one-step labeling method, it can suffer from nonspecific methylation side reactions. Furthermore, the 20-minute half-life for

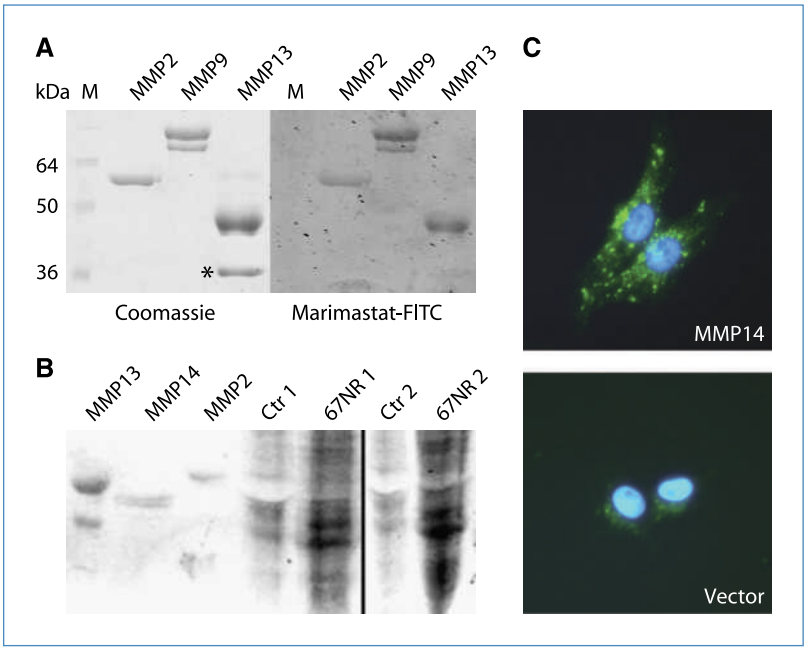

Figure 3. Specificity of labeled marimastat and *in vitro* imaging of MMPs. A, recombinant human MMPs 2, 9, and 13 were electrophoresed on SDS-PAGE, renatured, incubated with marimastat-FITC (**3**), and washed extensively. Subsequently, the same gel was stained with Coomassie brilliant blue. The asterisk indicates the hemopexin domain of MMP13. B, total protein lysates were prepared from two normal mammary glands (Ctr 1, Ctr 2) and two primary 67NR tumors (67NR 1, 67NR 2). Proteins (100 μg) were analyzed by SDS-PAGE, renatured, and labeled with marimastat-FITC (**3**) with 2 μg of recombinant human MMPs 2, 13, and 14 as standards. C, MDA-MB-231 cells stably transfected with MMP14 and vector were incubated with marimastat-FITC (**3**) (green). Cell nuclei were counterstained with Hoechst dye (blue).

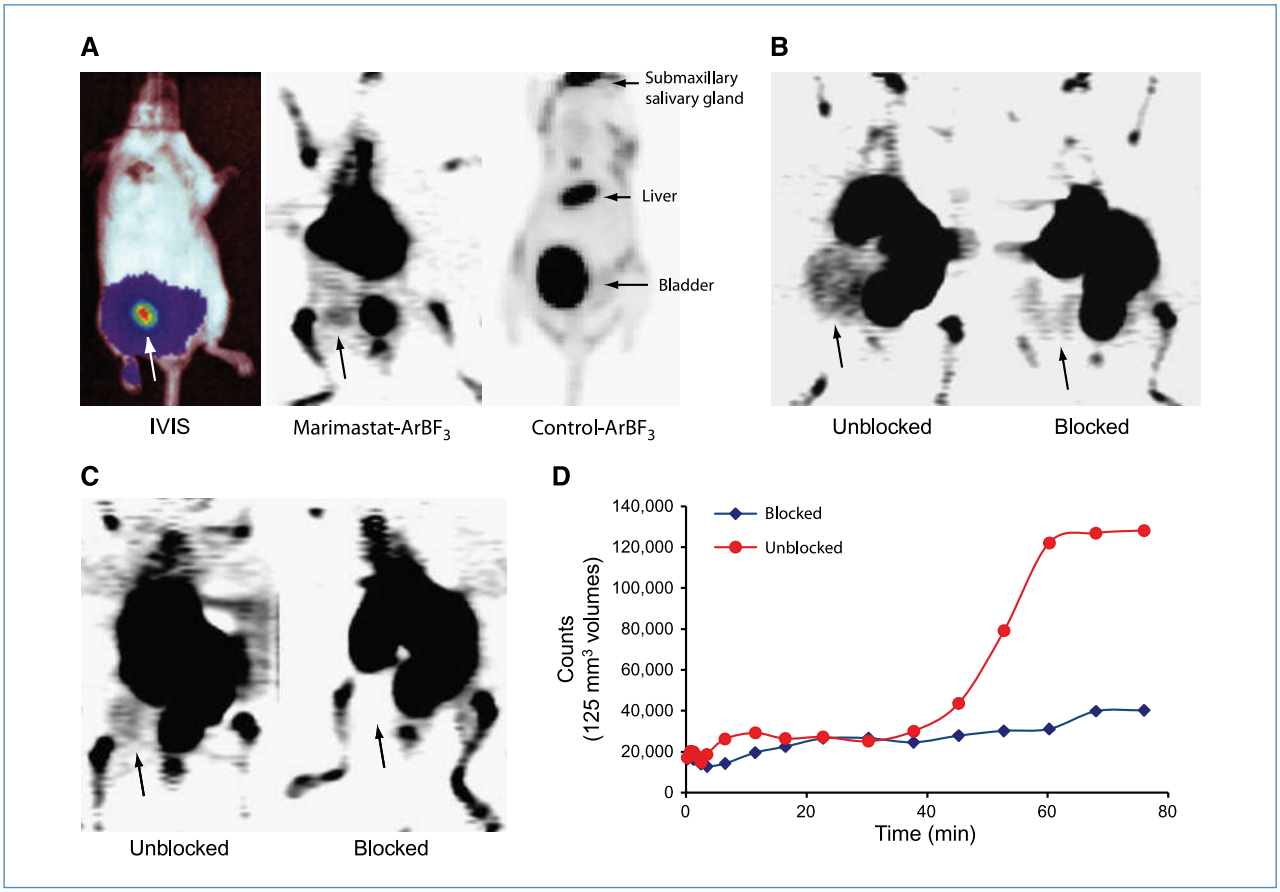

Figure 4. *In vivo* PET imaging of MMPs in murine breast carcinomas. A, IVIS image of 67NR/CMV-Luciferase derived primary tumor (left) is from the same mouse imaged next day by MicroPET with 50 μCi of marimastat-$ArBF_3$ (middle). Control mouse injected with 440 μCi control-$ArBF_3$ (right). Pictures were reconstructed from a scan taken 50 to 80 min after tracer injection. B, MicroPET images of 67NR breast tumor mice with 100 μCi of marimastat-$ArBF_3$ (**5**) injected either in an unblocked tumor mouse (left) or in a tumor mouse preblocked with 300 nmol of marimastat (right). C, biological replicate of B using tumors established on different dates and imaged on different days. D, time–activity curves of the primary tumor of unblocked and preblocked marimastat-$ArBF_3$ (**5**) injected 67NR mice, respectively.

C-11 dramatically reduces the imaging time window (19), therefore reducing image quality compared with ligands labeled with other PET isotopes (20). Our labeling technique captures the advantages of a single-step labeling in the case of F-18 to afford ligands with specific activities that are potentially useful for imaging.[7]

As this approach is conceptually very different from other radiolabeling methods, it is essential to briefly address some of the chemical attributes of an ^{18}F-labeled $ArBF_3$. The first is the question of chemical purity. Although labeling must proceed through mono- and difluoronated intermediates en route to the labeled $ArBF_3$, the mono- and difluoroboranes/boronates are unstable at pH 7 (21), and as such, the $ArBF_3$ is the only labeled species isolated. The second concern relates to specific activity. Although high specific activity is always preferable, there is no universally accepted value as to what minimal specific activity represents a threshold of utility and often a value of ~1 Ci/μmol is sufficient for imaging. Traditionally, radiosyntheses are performed under no carrier–added conditions to guarantee the highest possible specific activities. A prevailing misconception in such work is that no carrier–added fluoride has a specific activity close to that of carrier-free, that is, 1,720 Ci/μmol; in practice, however, the specific activity of "no carrier–added" [^{18}F]fluoride generally falls in the range of 3 to 10 Ci/μmol. As such, there is a significant amount of carrier [^{19}F]fluoride present in all no carrier–added syntheses. Furthermore, the decay that accompanies multistep radiosyntheses of mid-size molecules further reduces the final specific activities, which commonly fall in the range of 1 to 2 Ci/μmol, or less. Because three fluoride ions condense with one arylboronate to give an $ArBF_3$, the law of mass action ensures that the resulting $ArBF_3$ has a decay-corrected specific activity that is thrice that of the source fluoride; therefore, activities as high as 30 Ci/μmol may be envisaged if no carrier–added fluoride with a specific

[7] Li Y, Ting R, Harwig C, et al. Kit-like ^{18}F-labeling of small molecules with specific activities suitable for *in vivo* PET imaging: toward imaging cancer associated matrix metalloproteases. 2010; submitted for publication.

activity of 10 Ci/μmol is used. Nevertheless, yields may be low unless reaction volume is minimized; the use of 500 mCi of no carrier–added fluoride with a specific activity of 10 Ci/μmol represents 50 nmol total [$^{18/19}$F]fluoride, which if contained in 1 μL, would provide a 50 mmol/L fluoride solution that is high enough to afford reasonable yields in terms of an $ArBF_3$. Finally, because of the relatively high presence of carrier [^{19}F]fluoride that are present, even under no carrier–added conditions, statistically the labeled $ArBF_3$ will contain only one atom of [^{18}F]fluoride (3, 21).

Despite a relatively low signal to noise ratio, tumor-labeling was specific as shown from the unlabeled blocking control studies. Notably, image quality did not improve with higher specific activity probes; tumor images were similar irrespective of whether the specific activity of marimastat-$ArBF_3$ (**5**) was 0.185 Ci/μmol (Fig. 4B) or 0.39 Ci/μmol (Fig. 4C), corresponding to ~12 nmol/L or ~27 nmol/L *in vivo*. Because the respective concentrations of **5** were 3.5× and 10× the K_d, this suggests, but does not prove that even higher specific activities would not improve imaging quality. Although a slightly better image was recorded with higher specific activity (Fig. 4C), this improvement is ascribed to larger tumor size, as tumors on day 33 (Fig. 4C) were twice as large as those imaged on day 26 (Fig. 4B).

It has to be noted that previous studies using ^{18}F-conjugated MMP inhibitors for *in vivo* imaging also revealed high uptake of tracer in tissues with known nonpathologic MMP expression such as the liver (22, 23). Blood also contains MMPs. This is a particular problem for broad-spectrum MMP inhibitors and leads to poor target/nontarget contrasts when imaging disease tissues. With more data becoming available on the expression and activity of specific MMPs in particular pathologies, antibodies or small molecule inhibitors with narrow specificity can be developed and modified for the rapid conversion to ^{18}F-conjugated radiotracers using our novel one-step labeling chemistry. A promising target for this strategy is MMP13, which is highly expressed in human breast cancer (24), and for that, specific inhibitors are currently in active development (25).

Although the metabolic fate of marimastat-$ArBF_3$ (**5**) is unknown, we measured the inhibitory activity in the urine postmortem; the observed IC_{50} value per microcurie was comparable to that injected suggesting that **5** was not being metabolized and clears to the urine intact (Supplementary Fig. S2). Notably, the $ArBF_3$ control that is not appended to marimastat does not clear to the gut (Fig. 4A). This illustrates that clearance is at least partially governed by the marimastat moiety and points to potential clinical applications in the gastrointestinal tract, which experience high drug exposures.

The *in vivo* application of [^{18}F]marimastat-aryltrifluoroborate represents a key development in PET imaging as we have reduced to practice the production of a shelf-stable bioconjugate that can be rapidly labeled with [^{18}F]fluoride for PET imaging in a simple one-step aqueous reaction at ambient temperatures under mild conditions. The key to this advance in PET imaging is the synthesis of stable [^{18}F]aryltrifluoroborates as viable alternatives to [^{18}F]organofluorides. The use of a stable arylboronic acid as a captor of aqueous [^{18}F]fluoride avoids tedious multistep syntheses or harsh fluorination conditions. These findings should encourage the widespread development of new molecularly targeted ^{18}F-labeled peptidic and small molecule drugs for *in vivo* imaging. Hence, the first *in vivo* imaging of tumor metalloproteinases using marimastat as a scaffold indicates that labeling of other ligands is a facile approach for targeted PET imaging for human diagnosis as well as drug target validation, tissue targeting, and compound clearance to aid drug development.

Disclosure of Potential Conflicts of Interest

No potential conflicts of interest were disclosed.

Acknowledgments

We thank Siobhan McCormick for image processing, Salma Jivan for assistance in fluoride preparation, Rick Kornelsen, Gayle Smith, and Pamela Austin for tail vein injections, and Dr. Cal Roskelley for helpful discussions.

Grant Support

U. auf dem Keller was supported by a German Research Foundation (Deutsche Forschungsgemeinschaft) research fellowship. C.L. Bellac is supported by postdoctoral fellowships of the Swiss National Science Foundation and the Novartis Jubilee Foundation. P.F. Lange is supported by a Feodor Lynen Research Fellowship of the Alexander von Humboldt Foundation. R. Ting was a recipient of Michael Smith and Gladys Estella Laird Fellowships. D.M. Perrin was awarded a Michael Smith Senior Career Scholar Award and is supported by operating and PoP grants of the CIHR. C.M. Overall is supported by a Canada Research Chair in Metalloproteinase Proteomics and Systems Biology. This work was supported by a program project grant in Breast Cancer Metastases from the Canadian Breast Cancer Research Alliance with funds from the Canadian Breast Cancer Foundation and the Cancer Research Society (awarded to S. Dedhar, D.M. Perrin, and C.M. Overall) as well as with an Infrastructure Grant from the Michael Smith Foundation for Health Research.

The costs of publication of this article were defrayed in part by the payment of page charges. This article must therefore be hereby marked *advertisement* in accordance with 18 U.S.C. Section 1734 solely to indicate this fact.

Received 05/03/2010; revised 07/12/2010; accepted 08/04/2010; published OnlineFirst 08/20/2010.

References

1. Willmann JK, van Bruggen N, Dinkelborg LM, Gambhir SS. Molecular imaging in drug development. Nat Rev Drug Discov 2008;7:591–607.
2. Ting R, Adam MJ, Ruth TJ, Perrin DM. Arylfluoroborates and alkylfluorosilicates as potential PET imaging agents: high-yielding aqueous biomolecular 18F-labeling. J Am Chem Soc 2005;127:13094–5.
3. Ting R, Harwig C, auf dem Keller U, et al. Toward [^{18}F]-labeled aryltrifluoroborate radiotracers: *in vivo* positron emission tomography imaging of stable aryltrifluoroborate clearance in mice. J Am Chem Soc 2008;130:12045–55.
4. Coussens LM, Fingleton B, Matrisian LM. Matrix metalloproteinase inhibitors and cancer: trials and tribulations. Science 2002;295:2387–92.
5. Overall CM, Kleifeld O. Tumour microenvironment—opinion: validating matrix metalloproteinases as drug targets and anti-targets for cancer therapy. Nat Rev Cancer 2006;6:227–39.

6. Overall CM, Lopez-Otin C. Strategies for MMP inhibition in cancer: innovations for the post-trial era. Nat Rev Cancer 2002;2:657–72.
7. Whittaker M, Floyd CD, Brown P, Gearing AJ. Design and therapeutic application of matrix metalloproteinase inhibitors. Chem Rev 1999; 99:2735–76.
8. Tam EM, Morrison CJ, Wu YI, Stack MS, Overall CM. Membrane protease proteomics: isotope-coded affinity tag MS identification of undescribed MT1-matrix metalloproteinase substrates. Proc Natl Acad Sci U S A 2004;101:6917–22.
9. Tam EM, Wu YI, Butler GS, Stack MS, Overall CM. Collagen binding properties of the membrane type-1 matrix metalloproteinase (MT1-MMP) hemopexin C domain. The ectodomain of the 44-kDa autocatalytic product of MT1-MMP inhibits cell invasion by disrupting native type I collagen cleavage. J Biol Chem 2002; 277:39005–14.
10. Aslakson CJ, Miller FR. Selective events in the metastatic process defined by analysis of the sequential dissemination of subpopulations of a mouse mammary tumor. Cancer Res 1992;52:1399–405.
11. Lou Y, Preobrazhenska O, auf dem Keller U, et al. Epithelial-mesenchymal transition (EMT) is not sufficient for spontaneous murine breast cancer metastasis. Dev Dyn 2008;237:2755–68.
12. Kappelhoff R, auf dem Keller U, Overall CM. Analysis of the degradome with the CLIP-CHIP microarray. Methods Mol Biol 2010;622:175–93.
13. Butler GS, Tam EM, Overall CM. The canonical methionine 392 of matrix metalloproteinase 2 (gelatinase A) is not required for catalytic efficiency or structural integrity: probing the role of the methionine-turn in the metzincin metalloprotease superfamily. J Biol Chem 2004; 279:15615–20.
14. Saghatelian A, Jessani N, Joseph A, Humphrey M, Cravatt BF. Activity-based probes for the proteomic profiling of metalloproteases. Proc Natl Acad Sci U S A 2004;101:10000–5.
15. Minn AJ, Gupta GP, Siegel PM, et al. Genes that mediate breast cancer metastasis to lung. Nature 2005;436:518–24.
16. Bravo-Cordero JJ, Marrero-Diaz R, Megias D, et al. MT1-MMP pro-invasive activity is regulated by a novel Rab8-dependent exocytic pathway. EMBO J 2007;26:1499–510.
17. Bremer C, Tung CH, Weissleder R. *In vivo* molecular target assessment of matrix metalloproteinase inhibition. Nat Med 2001;7:743–8.
18. Paulick MG, Bogyo M. Application of activity-based probes to the study of enzymes involved in cancer progression. Curr Opin Genet Dev 2008;18:97–106.
19. Zheng QH, Fei X, Liu X, et al. Comparative studies of potential cancer biomarkers carbon-11 labeled MMP inhibitors (S)-2-(4′-[^{11}C]methoxybiphenyl-4-sulfonylamino)-3-methylbutyric acid and *N*-hydroxy-(R)-2-[[(4′-[^{11}C]methoxyphenyl)sulfonyl]benzylamino]-3-methylbutanamide. Nucl Med Biol 2004;31:77–85.
20. Van de Wiele C, Oltenfreiter R. Imaging probes targeting matrix metalloproteinases. Cancer Biother Radiopharm 2006;21:409–17.
21. Ting R, Harwig CW, Lo J, et al. Substituent effects on aryltrifluoroborate solvolysis in water: implications for Suzuki-Miyaura coupling and the design of stable (18)F-labeled aryltrifluoroborates for use in PET imaging. J Org Chem 2008;73:4662–70.
22. Wagner S, Breyholz HJ, Holtke C, et al. A new 18F-labelled derivative of the MMP inhibitor CGS 27023A for PET: radiosynthesis and initial small-animal PET studies. Appl Radiat Isot 2009;67:606–10.
23. Furumoto S, Takashima K, Kubota K, Ido T, Iwata R, Fukuda H. Tumor detection using 18F-labeled matrix metalloproteinase-2 inhibitor. Nucl Med Biol 2003;30:119–25.
24. Freije JM, Diez-Itza I, Balbin M, et al. Molecular cloning and expression of collagenase-3, a novel human matrix metalloproteinase produced by breast carcinomas. J Biol Chem 1994;269:16766–73.
25. Li JJ, Johnson AR. Selective MMP13 inhibitors. Med Res Rev 2010 Mar 1 [Epub ahead of print].